

# Content-Based Detection of Temporal Metadata Manipulation

Rafael Padilha<sup>1</sup>✉, Tawfiq Salem<sup>2</sup>, Scott Workman<sup>3</sup>,  
Fernanda A. Andaló<sup>1</sup>, Anderson Rocha<sup>1</sup>, Nathan Jacobs<sup>4</sup>

<sup>1</sup> University of Campinas, Brazil

<sup>2</sup> Purdue University, USA

<sup>3</sup> DZYNE Technologies, USA

<sup>4</sup> University of Kentucky, USA

✉ rafael.padilha@ic.unicamp.br

## Abstract

Most pictures shared online are accompanied by a temporal context (i.e., the moment they were taken) that aids their understanding and the history behind them. Claiming that these images were captured in a different moment can be misleading and help to convey a distorted version of reality. In this work, we present the nascent problem of detecting timestamp manipulation. We propose an end-to-end approach to verify whether the purported time of capture of an image is consistent with its content and geographic location. The central idea is the use of supervised consistency verification, in which we predict the probability that the image content, capture time, and geographical location are consistent. We also include a pair of auxiliary tasks, which can be used to explain the network decision. Our approach improves upon previous work on a large benchmark dataset, increasing the classification accuracy from 59.03% to 81.07%. Finally, an ablation study highlights the importance of various components of the method, showing what types of tampering are detectable using our approach.

## 1. Introduction

With the popularization of social networks and advances in image capturing devices during the last decade, the number of images shared online has grown exponentially. Their increasing availability coupled with easy-to-use photo editing software has resulted in a profusion of manipulated images. Such images are often maliciously used to support false claims and opinions. Consequently, the research community has explored many approaches to detect image content tampering [4, 12, 35]. Even though visual manipulation is now well-understood and reasonably explored in the lit-

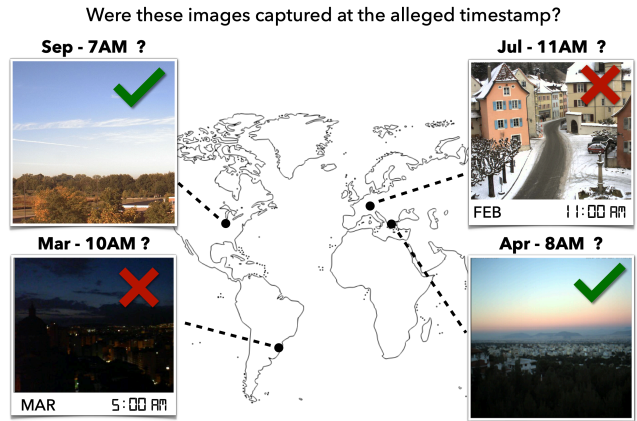


Figure 1. Our goal is to analyze if an alleged timestamp is consistent with the visual information present in a photograph. It is essential to consider the appearance of the scene (e.g., illumination and weather conditions) as well as the location of the photograph when verifying a timestamp.

erature, there is a more subtle type of manipulation that still has been relatively unexplored by the research community: *timestamp manipulation*.

Presenting an image as if it was captured in a different moment in time can corroborate a false narrative and spread misinformation. Recent examples include the “Fishwrap” campaign [10], an online campaign that shared terror news articles from past years in an attempt to spread fear and uncertainty. In cases like this, articles often contain unaltered pictures that are displaced in time to validate a false story. Even though the timestamp of an image might be stored in its metadata when the photo was originally taken, it can be easily tampered with by freely available metadata editors (e.g., EXIF Date Changer Lite or Metadata++).

In this sense, it is important to develop methods capable

of verifying the consistency between the visual information of a picture and its timestamp. This is a challenging task that requires a deep understanding of the scene, as its appearance may vary depending on the hour of the day, month of the year, and the location where the photo was taken (Figure 1). Moreover, factors such as the weather, lighting conditions, device quality, and depicted elements influence the appearance of a recorded scene and directly affect our perception of time. Existing methods often estimate indirect features from the image content, such as the sun position in the sky [3, 15, 19] or meteorological measures [3], and contrast them to registered values for the same day, hour and location. However, these are limited cues which may not always be sufficient nor easily available.

We propose a convolutional neural network (CNN) architecture that analyzes a ground-level image and a claimed timestamp, receiving as additional context for its decision the geographic coordinates and a satellite image of that location. Our model is optimized in an end-to-end manner using a multi-task loss function, with the main goal of checking for manipulations and an auxiliary objective of estimating transient attributes [17] (i.e., high-level properties of the scene appearance, such as *snow*, *dusk* or *gloomy*). This secondary task introduces an explainability component to our model, aiding in understanding its decisions. We evaluate the proposed approach both quantitatively and qualitatively, achieving state-of-the-art results on a reference benchmark dataset [24].

#### The contributions of our work include:

- A new method for verifying the timestamp of an image by comparing the appearance of the scene with time, location, and satellite imagery.
- A comprehensive ablation study of the impact of each input modality and backbone architecture to help us understand when the method works and fails.
- A high-level exploration of which elements in a scene might indicate timestamp inconsistency.
- A demonstration of how to use our method for estimating a possible time-of-capture, in scenarios in which the timestamp is missing from the metadata.

## 2. Related Work

The analysis of temporal information has been explored in different ways in the literature. In this section, we review relevant methods that approach this problem.

### 2.1. Metadata Tampering Detection

Traditionally, most tampering detection techniques focus on image content manipulation, with only a few recent

works approaching metadata tampering detection. To check the integrity of the geographic location, researchers borrow ideas extensively from the image retrieval and landmark recognition literature [8, 21, 23, 31], focusing on identifying visual elements in the scene and matching them with large-scale databases of geo-tagged images.

Considering timestamp manipulation, Kakar et al. [15] and Li et al. [19] propose to verify the timestamp by estimating the sun azimuth angle from shadow angles and sky appearance, comparing it to the sun position calculated from the image metadata. Chen et al. [3] optimize a CNN to jointly estimate temperature, humidity, sun altitude angle and weather condition from an input image, comparing them with meteorological data registered from the day and time stored in its metadata. In [2], the authors approach this task as an event identification problem: they train a CNN with images from a specific event (i.e., sharing similar location and timestamp) to determine whether a test image, presumably sharing the same metadata, belongs to that event. Differently from them, we aim at directly verifying whether a claimed time-of-capture is *consistent* with the visual content of an image, independent of particular visual cues and without the need to optimize for a specific event.

Salem et al. [24] learn a dynamic map of visual attributes that captures the relationship between location, time, and the expected appearance of a photograph. Their approach predicts visual attributes from a combination of satellite imagery, time, and geographic location. To apply the method to metadata verification, these attributes are compared to similar information extracted from a ground-level picture, computing a distance metric and using it as a consistency score to detect if a timestamp has been tampered. In a similar manner, we train a global model that captures how visual appearance relates to location and time. However, we specifically focus on contrasting an alleged timestamp against the visual characteristics of a picture by directly optimizing for this task.

### 2.2. Time-of-capture Estimation

Approaching the problem from a different perspective, we also analyze methods for directly estimating time-of-capture, with time-scales ranging from hours to decades. Several works leverage specific visual elements as cues to date pictures, such as human appearance and fashion [7, 25], visual style of objects [14, 29], architecture styles [18], sun position [15, 19, 28], and photo-generation artifacts [6, 20, 22].

Despite their impressive results, these methods require the presence of particular visual elements in a scene to reliably estimate time. In their absence, a different class of methods should be considered. In this sense, a line of research closely related to this work explores how the global appearance of a scene changes over time.

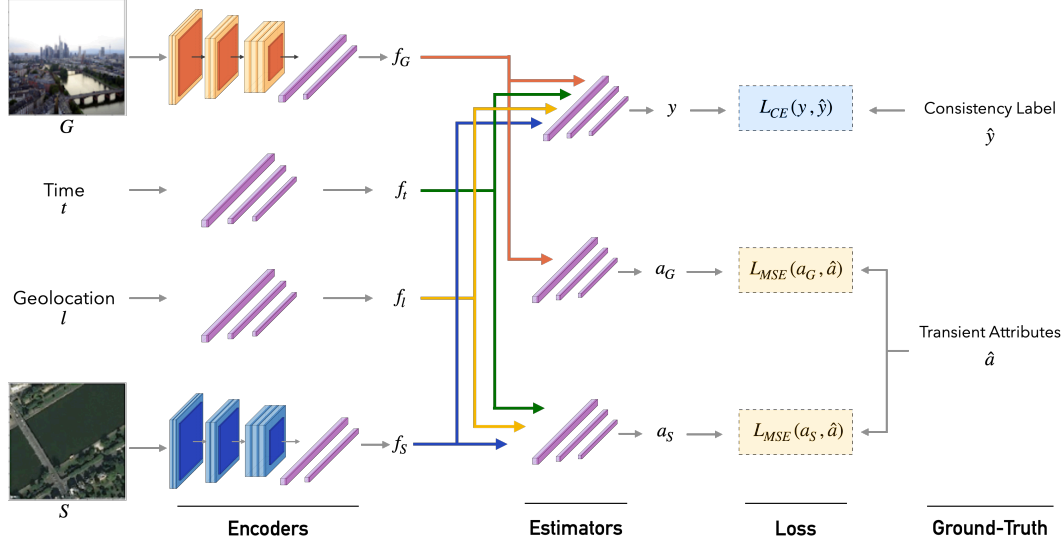


Figure 2. An overview of our approach. Ground-level image  $G$ , timestamp  $t$ , geo-coordinates  $l$  and satellite image  $S$  have their features extracted by encoder networks, and then fed to task-specific branches. One branch predicts the consistency label  $y$ , while auxiliary branches estimate transient attributes  $a_G$  and  $a_S$ . The network is optimized by a combination of cross-entropy and mean squared error losses. At inference time, the consistency answer  $y$  is considered for the tampering detection, while  $a_G$  and  $a_S$  offer insights about the decision of the network.

Volokitin et al. [30] use data-driven features to infer the time of the year and hour of the day of an outdoor scene. Some works [1, 17] aim to estimate transient attributes of a scene that inherently carry some degree of temporal information, such as season, weather, and illumination conditions. By combining the visual content with geographical information in the pretext task of time-of-capture estimation, Zhai et al. [33] learn a representation with high correlation to transient attributes.

This work builds upon these strategies, incorporating visual information from ground-level photo, satellite imagery, and geographical coordinates to check for time-of-capture consistency. Even though our goal is not to explicitly estimate when an image was taken, we show how our method can be applied for cases in which the timestamp is missing.

### 3. Proposed Method

Our goal is to assess if the visual content of an image is consistent with its time-of-capture. For this, our method must extract discriminative features from the scene appearance and contrast them with the expected appearance for that specific time-of-capture. As variations in appearance over time are highly dependent on the location of the scene, it is essential to provide, as additional context, geographic cues of where the picture was taken [24, 33].

With this in mind, we propose a CNN architecture (Figure 2) to estimate the probability  $P(y|G, t, S, l)$  that a given ground-level image  $G$ , associated with location  $l$  and satellite image  $S$ , is consistent ( $y = 0$ ) or inconsistent

( $y = 1$ ) with an alleged timestamp  $t$ . By providing location  $l$  as input, the network will be able to consider the influence of geographic position in seasonal patterns (e.g., winter months in the Northern hemisphere with reduced sunlight hours, and the opposite in the Southern hemisphere). Moreover, satellite image  $S$  provides an additional context, such as whether the image was captured in an urban or rural area. As such elements are not time-dependent, we assume  $S$  is linked to the location  $l$  but not with timestamp  $t$ , avoiding the need for a satellite image at the precise time-of-capture being checked.

For explainability, the network also estimates transient attributes  $a_G$  and  $a_S$ . These are 40-dimensional arrays, with each value encoding the presence of a characteristic of scene appearance (e.g., fog, hot, beautiful, summer) to the interval  $[0, 1]$ . The attributes  $a_G$  are estimated solely from the ground-level image and capture the high-level properties of the scene at the moment it was recorded. In contrast,  $a_S$  is estimated from the satellite photo, location coordinates, and the alleged timestamp, and can be interpreted as a prediction of the expected scene appearance at the alleged moment.

#### 3.1. Network Architecture

Each input  $G, t, l, S$  is processed by individual sub-networks, responsible for extracting characteristics from each modality and encoding them into 128-dimensional feature vectors.

**Visual Encoder.** Both the ground-level and satellite

images,  $G$  and  $S$ , are processed by a backbone CNN, extracting feature maps from the last convolutional layer. The feature maps are then processed by two additional fully connected layers, with 256 and 128 units respectively, each followed by a ReLU activation and batch normalization, resulting in feature vectors  $f_G$  and  $f_S$ .

**Location and Time Encoder.** We represent the location  $l$  in earth-centered earth-fixed (ECEF) coordinates, scaled to  $[-1, 1]$ ; whereas time  $t$  is represented by the month and hour of the day (UTC) scaled to  $[-1, 1]$ . Both sub-networks share similar architectures, comprised of three fully connected layers, with 256, 512 and 128 neurons respectively, each followed by a ReLU activation function and batch normalization, resulting in feature vectors  $f_l$  and  $f_t$ .

**Task-specific Branches.** Once each feature  $f_G$ ,  $f_S$ ,  $f_l$  and  $f_t$  has been extracted, they are fed to task-specific branches. Each branch consists of three fully connected layers. The initial two have 256 and 512 units respectively, followed by ReLU and batch normalization, while the third maps the intermediate features to the output dimension of each task. One branch receives the concatenation of  $\{f_G, f_S, f_l, f_t\}$  and outputs the consistency  $y$ . Its last fully connected layer has two units followed by a softmax operation, allowing us to interpret the output as the probability  $P(y | G, t, S, l)$ . Another branch receives as input  $f_G$  and outputs a set of transient attributes  $a_G$ . Likewise, a third branch processes the concatenation of  $\{f_S, f_l, f_t\}$  and outputs attributes  $a_S$ . Their final dense layers have a number of neurons matching the quantity of estimated transient attributes  $|\hat{a}|$  (in our experiments,  $|\hat{a}| = 40$ ), followed by a sigmoid activation.

### 3.2. Loss Function

Our network is optimized in an end-to-end manner both for timestamp consistency and transient attribute estimation tasks. Even though the main goal is tampering detection, the auxiliary tasks allow our model to predict properties of the scene, separately considering the alleged timestamp or the ground-level visual information. Both sets of attributes can be compared, offering insights about the model decision.

For the consistency verification branch, we calculate the binary cross-entropy loss:

$$L_{CE}(y, \hat{y}) = -\hat{y} \log(y) - (1 - \hat{y}) \log(1 - y) \quad (1)$$

between the consistency prediction  $y$  and the ground-truth  $\hat{y}$ . For the transient attribute branches, we compute the mean squared error between estimated transient attributes  $a$  and ground-truth  $\hat{a}$ :

$$L_{MSE}(a, \hat{a}) = \frac{1}{|\hat{a}|} \sum_{i=1}^{|\hat{a}|} (a_i - \hat{a}_i)^2. \quad (2)$$

We compute two separate  $L_{MSE}$  terms with respect to  $a_G$  and  $a_S$ . By doing so, the model learns to extract the transient attributes directly from the ground-level image, while also being able to estimate them from the satellite photo, location coordinates and given timestamp. Finally, the whole network is jointly optimized to minimize their sum:

$$L = L_{CE}(y, \hat{y}) + L_{MSE}(a_G, \hat{a}) + L_{MSE}(a_S, \hat{a}). \quad (3)$$

## 4. Experimental Analysis

We evaluated our method for tampering detection, in which it outputs whether the timestamp is consistent with the visual attributes of the ground-level image. We performed an ablation study of the different input modalities, as well as of the backbone CNNs used as visual encoders. We assessed the quality of our method considering the accuracy and ROC curves in the tampering detection and performed additional experiments to investigate its robustness.

### 4.1. Dataset and Training Details

We used the Cross-View Time dataset [24], comprising more than 300k ground-level images. The dataset combines 98k images from 50 static outdoor webcams of the Archive of Many Outdoor Scenes [13], and 206k geotagged smartphone pictures from the Yahoo Flickr Creative Commons 100 Million Dataset [27]. Ground-level images were captured worldwide in different hours of the day and months throughout the year, and are associated with geographical coordinates, timestamp (UTC) and a co-located satellite image. We employed the same data splits provided by the authors, training on 280k images and testing on 25k.

For training, batches were randomly sampled from the training images, with corresponding timestamp, geo-coordinates and satellite image. For each consistent sample, we generated a tampered version by exchanging its timestamp to that of a random image in the training set. Therefore, training batches were composed of the same number of consistent and inconsistent tuples. At test time, a similar process was used, generating a tampered tuple for each available test image.<sup>1</sup>

We use a VGG-16 [26] network pre-trained on *Places* dataset [34] as the feature extractor for the ground-level image, while a ResNet-50 [9] network pre-trained on *ImageNet* [5] processes the satellite image. This is a similar architecture to [24] which allows a fair comparison to their method. Before being processed by the networks, we resize  $G$  and  $S$  to  $224 \times 224$  and scale each pixel to  $[-1, 1]$ .

Our architecture was optimized using Adam [16] with an initial learning rate of  $10^{-5}$ , batches of 32 images, and training lasts 30 epochs. When calculating the loss for a batch, only real tuples were considered in computing the

<sup>1</sup>The same seed was selected for all experiments and the tampered timestamps of test images will be made publicly available.



Table 1. Results for the ablation study of input modalities and visual encoder architectures.

Modalities	VGG-16 / ResNet-50		ResNet-50		DenseNet-121	
	Acc (%)	AUC	Acc (%)	AUC	Acc (%)	AUC
G, t	63.61	0.699	65.30	0.744	67.53	0.766
G, t, S	72.06	0.813	74.94	0.851	77.03	0.855
G, t, l	<b>77.93</b>	<b>0.853</b>	75.05	0.852	78.73	0.873
G, t, l, S	76.09	0.847	78.35	<b>0.877</b>	80.47	0.880
G, t, l, S (TA)	75.71	0.834	<b>78.68</b>	0.865	<b>81.07</b>	<b>0.885</b>
Salem et al. [24]	59.03	0.627	—	—	—	—

$L_{\text{MSE}}$  terms of Equation 3, as the ground-truth transient attributes for tampered timestamps are not available. With the exception of VGG-16 and ResNet-50 sub-networks, the weights of convolutional and fully connected layers were initialized with Xavier initialization, and we applied  $L_2$  regularization ( $\lambda = 0.001$ ).

## 4.2. Ablation Study

Each input modality influences the performance of the timestamp tampering detection. We performed an ablation study, considering the impact of location  $l$  and satellite image  $S$ , given as additional context to the ground-level image  $G$  and timestamp  $t$ . To better evaluate the impact of each modality, we optimized the models considering solely the consistency verification, i.e., by removing the mean-squared error terms from Equation 3.

We compared our models with the method proposed by Salem et al. [24], using the same weights and choice of hyperparameters provided by the authors. They employed a similar architecture to ours—with VGG-16 and ResNet-50 as feature extractors for the ground-level and satellite imagery, respectively—allowing us for a fair comparison between both approaches.

We also considered variations of our architecture in which we use a ResNet-50 [9] or a DenseNet-121 [11] as encoders for both ground-level and satellite images. In this scenario, even though the branches are similar, they do not share weights as each processes a different type of input.

Finally, considering all input modalities and evaluated backbones, we optimized the model with the transient attribute estimation task, by employing the complete loss function from Equation 3. We present the accuracy, the ROC curves, and the area under them (AUC) for our evaluation in Table 1 and Figure 3.

Our results show that optimizing a method specifically for this task was essential to better detect timestamp manipulation, surpassing Salem et al. [24] even when only ground-level image  $G$  and timestamp  $t$  are present. Besides that, including geographical information considerably

improved performance, as the model learns how shifts in latitude and longitude correlate to the expected appearance of a scene and an alleged timestamp (e.g., a snowy scene in December might be consistent if taken in the Northern hemisphere, but less so in the Southern hemisphere). Similarly, satellite imagery boosts performance, as this modality complements the ground-level information, allowing the network to better learn the characteristics of the scene.

Replacing the backbone CNNs to ResNet-50 or DenseNet-121 improved the results even further. Even though VGG-16 is frequently used when performing transfer learning, the other architectures include several operations—such as residual learning and batch normalization—that boost optimization and performance. We achieve an accuracy of 81.07%, an improvement of 22 percentage points over Salem et al. [24].

Finally, the addition of the auxiliary optimization tasks— $G$ ,  $t$ ,  $l$ ,  $S$  (TA) in Table 1—slightly improved the results for the ResNet-50 and DenseNet-121 setups. Even though the estimated attributes,  $a_G$  and  $a_S$ , are not considered when determining if tampering occurred, in Section 4.4 we use them to produce a simple explanation of the network’s decision.

## 4.3. Range of Tampering

In real scenarios, when the timestamp of a photograph is modified, the new time-of-capture is typically selected considering a plausible, often close to the original, moment in time as a way to make the detection harder. For example, claiming a 9AM image was captured in daylight hours is more convincing than saying it was captured at night.

To evaluate this scenario, we performed several experiments in which all images in our test set were tampered by an equal month and hour shift in both directions to its original time-of-capture. For a given shift pair  $(\Delta t_{\text{month}}, \Delta t_{\text{hour}})$ , we tampered every testing image by adding  $\pm \Delta t_{\text{month}}$  and  $\pm \Delta t_{\text{hour}}$  to its time of capture, effectively producing four tampered versions for each image. For example, for  $\Delta t_{\text{month}} = 1$  and  $\Delta t_{\text{hour}} = 2$ , a pic-

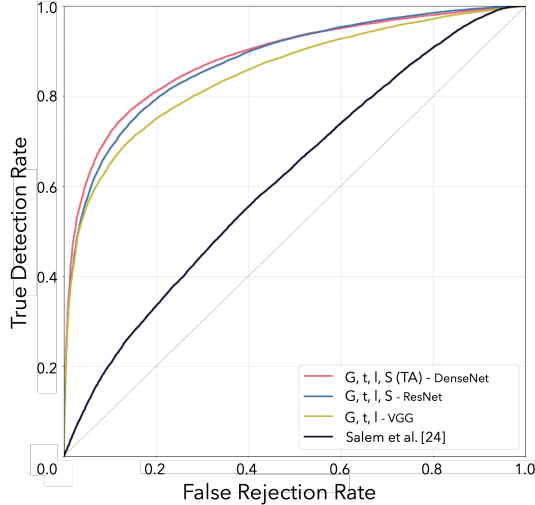


Figure 3. ROC curves for the best model of each backbone architecture in the ablation study, in comparison to [24].

ture captured in (Dec, 11AM) would generate timestamps (Jan, 9AM), (Jan, 1PM), (Nov, 9AM) and (Nov, 1PM). We evaluated the detection rate of such tampered images and present the results in Figure 4.

As we expected, the closer an alleged timestamp is to the original moment of capture, the harder it is to detect that tampering occurred. Shifts by a single hour or month were detected in less than 20% of the cases, probably due to the similarity in the appearance of the scene. However, as the gap between them increases, the inconsistency between time and visual appearance becomes more apparent and easily detectable. Interestingly, images that were presented as being captured in a different season ( $\Delta t_{month} \geq 3$ ) or period of the day ( $\Delta t_{hour} \geq 6$ , such as claiming a morning scene was captured at noon or during the night) were detected in more than 75% of the cases.

Additionally, we explored the sensitivity of our method to changes in the appearance of a scene, under fixed alleged timestamps. In a first evaluation, we selected images from different hours of the day, all taken in a particular month at the same location. Whereas, in a second experiment we employed images taken at the same hour and location but in different months. We computed the consistency probability of each image under fixed alleged timestamps, and plot the resulting curves in Figure 5. By doing so, we investigate how confident the network is that an alleged timestamp is consistent as time progresses in a scene.

The model correctly predicts high probabilities for images taken around the alleged timestamp, as seen by the peaks in the curves from Figure 5(a). Despite that, nighttime images tend to be very similar due to the lack of changes in illumination, reflecting in higher consistency probabilities between 9PM and 4AM. Similarly, Figure 5(b)

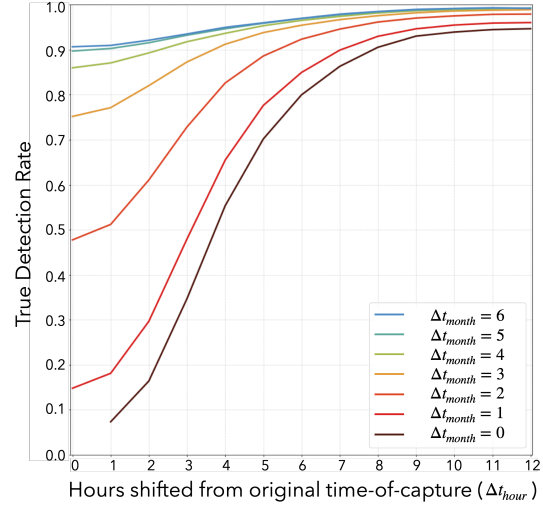


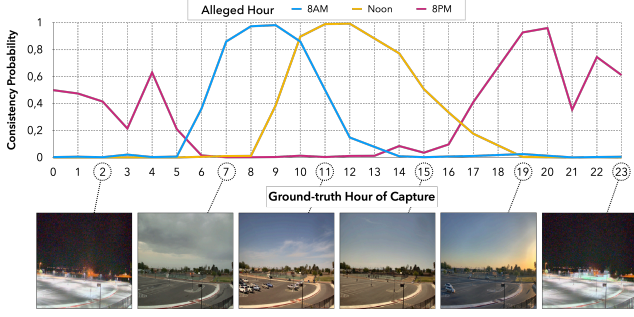
Figure 4. Detection rate for hour and month shifts from the original timestamp.

shows that our model also captured seasonal patterns, such as the variation in sunset hours across the year, even though monthly variations in the appearance of a scene tend to be smoother across neighboring months.

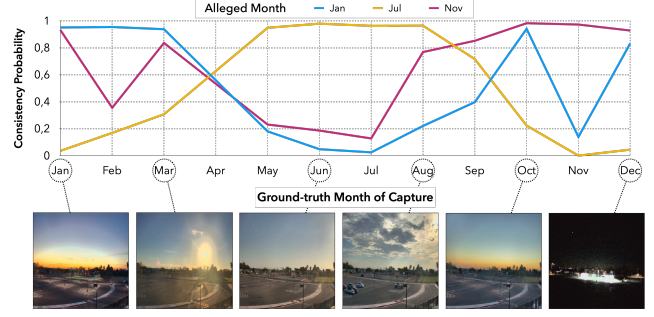
#### 4.4. Summer Snow and Midnight Sun: Tampering Telltales

As humans, we have a good intuition of which elements in a scene might be inconsistent with an alleged time-of-capture. For example, we can easily spot the inconsistency of a bright sky in a nighttime picture or of snow-covered ground in a summer scene. Besides achieving high accuracy in tampering detection, we wanted to provide simple explanations of what elements in the scene might be the cause of inconsistency according to our models. To this end, we investigated which image regions have the most impact on the decision of the network for both consistent and inconsistent examples. Similarly to [32], we occluded, in a sliding window manner, parts of the input image with gray patches of sizes  $50 \times 50$ ,  $100 \times 100$ ,  $100 \times 50$  and  $50 \times 100$  and evaluated the difference in consistency probability  $y$ . When an important area of a consistent image is occluded, we expect that  $y$  decreases; whereas, occlusions over an inconsistent sample might increase  $y$ , as it might hide discrepant elements. We present in Figure 6(a) the occlusion maps for two ground-level images, considering the ground-truth and manipulated timestamps. Additional examples are presented in the supplementary material.

The network focuses on specific elements depending on the time-of-capture being examined. When claiming the picture was captured in a different moment of the day, the model often considers regions spread across the image, as the scene changes uniformly with the shift in illumina-



(a) Same location recorded in April under different hours of the day.



(b) Same location recorded at 6PM in different months of the year.

Figure 5. Consistency probability for a scene recorded in varied moments in time. Each curve represents a fixed alleged timestamp being verified against ground-level images captured in different (a) hours of the day in April and (b) months of the year at 6PM. Our model captures several temporal patterns, identifying how the appearance of the scene changes according to the period of the day and season.

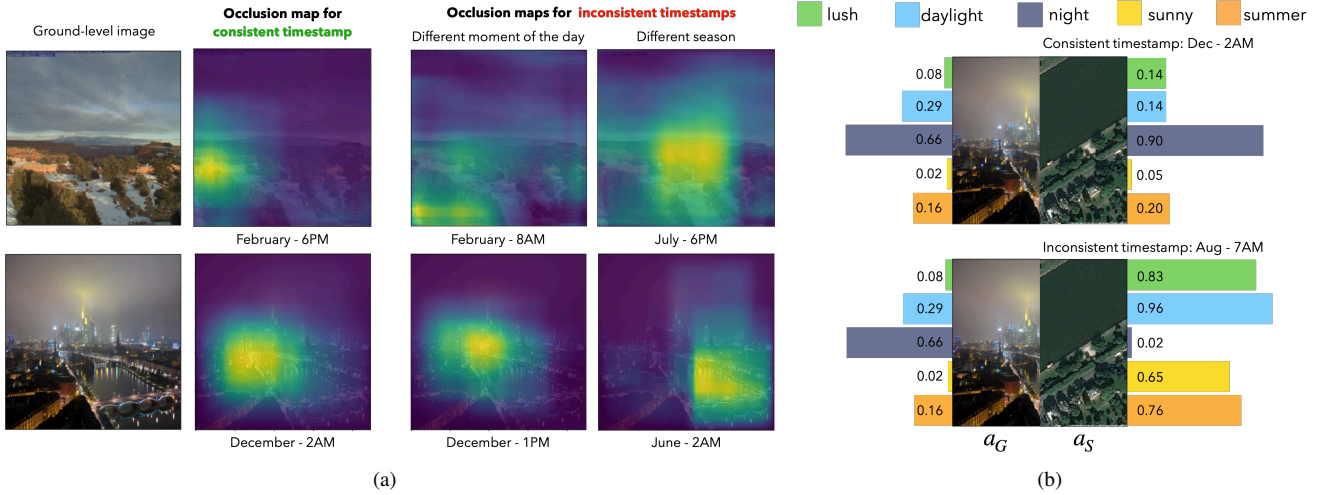


Figure 6. (a) Occlusion activation maps [32] for two pictures under different timestamps. The network focuses on specific elements depending on the alleged timestamp, with yellow regions representing important elements and blue areas having low impact for the decision. (b) Comparison between a subset of transient attributes  $a_G$  and  $a_S$  for a scene, for consistent (top) and inconsistent (bottom) timestamps. As the model estimates  $a_S$  without using ground-level signal, it greatly differs from  $a_G$  for inconsistent time-of-capture.

tion. Besides that, it also activates for some inconsistent elements, such as shadows (bottom-left corner of top example) and nighttime city lights (bottom example). Similarly, when tampering the month of both scenes, it considers background vegetation and lights reflected by the water, in the top and bottom scenes respectively.

Besides the occlusion maps, the transient attributes ( $a_G$  and  $a_S$ ) could provide additional evidence for the network decision. As  $a_G$  is obtained strictly from the ground-level image and is not influenced by a possibly manipulated timestamp, it captures the characteristics of the scene when the picture was taken. Differently,  $a_S$  is predicted from the satellite photo, location coordinates and the alleged timestamp, predicting the expected scene appearance at that alleged moment. In this sense, in case the timestamp  $t$  matches the ground-truth moment-of-capture, we expect  $a_G$  and  $a_S$  to be similar, whereas an inconsistent  $t$  might

lead to discrepancies in both sets of attributes.

We compare the sets of transient attributes for the nighttime skyline scene from Figure 6(a). We extracted attributes  $a_S$  considering two timestamps, one matching the ground-truth time-of-capture (December, 2AM) and another from a tampered timestamp (August, 7AM). We present in Figure 6(b) their comparison against  $a_G$ . To highlight their differences, we selected the top five divergent attributes from the inconsistent setup.

When considering the same moment in time,  $a_G$  and  $a_S$  tend to be similar, while an inconsistent timestamp will produce discrepant transient attributes. For the inconsistent example of Figure 6(b), our model expected it to be a sunny day of summer for the (August, 7AM) time-of-capture, in contrast to the nighttime scene in the ground-level image.

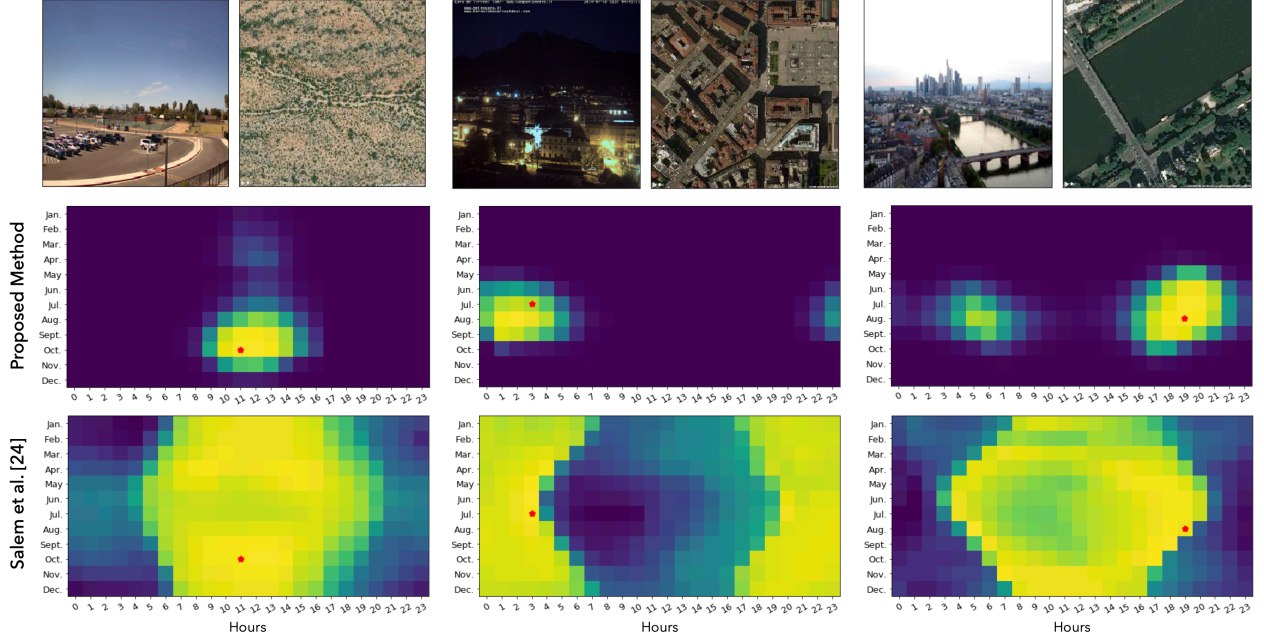


Figure 7. Heatmap of consistency probability distribution over local time (all possible months and hours of capture) for proposed method, in comparison to Salem et al. [24]. For each example, we show the ground-level picture and satellite image of that location. Yellow areas represent high consistency and blue indicates inconsistent moments in time. The red dot marks the ground-truth moment-of-capture.

#### 4.5. Time Estimation: A Qualitative Exploration

We also investigated the application of our method when a timestamp is not available. For a ground-level photo with associated location and satellite image, we predicted the consistency probability  $P(y|G, t_i, l, S), \forall t_i \in T$ , with  $T$  being all combinations of month and hour of capture.

In Figure 7, we show the consistency distribution heatmap for a few examples, as well as their ground-truth timestamp. In comparison, we generate heatmaps with the method from Salem et al. [24], computing the consistency score for all possible timestamps in a similar manner to Section 4.2. Even though our method is not explicitly trained to predict time, it is able to coherently estimate a possible span in which an image might have been captured. As it properly learned the influence of time in the appearance of a scene, capturing intrinsic temporal patterns, it also produces more precise estimations than [24].

## 5. Conclusion

We introduced a novel approach for detecting if the purported capture time of an image has been manipulated. Our architecture incorporates inputs from location, time, and satellite imagery, and is jointly optimized to detect timestamp tampering and estimate high-level attributes about the scene appearance. We demonstrated that each of these inputs is important for achieving high detection accuracy, improving the state-of-the-art on a large-scale dataset. We also

showed how to generate simple explanations for the classification decisions, as well how our method could estimate when an image was captured. Just like location and satellite imagery, our method could be easily adapted to receive other types of data as additional context. High-quality information, such as meteorological data similar to [3] or scene classification [34], could complement present features and improve tampering detection at the cost of increasing the computational burden. In future work, we will incorporate such additional data, as well as explicitly tackle the problem of estimating the time-of-capture of a photograph.

## References

- [1] Ryan Baltenberger, Menghua Zhai, Connor Greenwell, Scott Workman, and Nathan Jacobs. A fast method for estimating transient scene attributes. *IEEE Winter Conference on Applications of Computer Vision (WACV)*, 2016. 3
- [2] Bor-Chun Chen and Larry S Davis. Deep representation learning for metadata verification. In *IEEE Winter Conference on Applications of Computer Vision (WACV)*, pages 73–82, 2019. 2
- [3] Bor-Chun Chen, Pallabi Ghosh, Vlad I Morariu, and Larry S Davis. Detection of metadata tampering through discrepancy between image content and metadata using multi-task deep learning. In *IEEE Conference on Computer Vision and Pattern Recognition Workshops (CVPRW)*, pages 60–68, 2017. 2, 8
- [4] Vincent Cristlein, Christian Riess, Johannes Jordan, Corinna Riess, and Elli Angelopoulou. An evaluation of popular



- copy-move forgery detection approaches. *IEEE Transactions on Information Forensics and Security (TIFS)*, 7(6):1841–1854, 2012. 1
- [5] Jia Deng, Wei Dong, Richard Socher, Li-Jia Li, Kai Li, and Li Fei-Fei. Imagenet: A large-scale hierarchical image database. In *IEEE Conference on Computer Vision and Pattern Recognition (CVPR)*, pages 248–255, 2009. 4
- [6] Basura Fernando, Damien Muselet, Rahat Khan, and Tinne Tuytelaars. Color features for dating historical color images. In *IEEE International Conference on Image Processing (ICIP)*, pages 2589–2593, 2014. 2
- [7] Shiry Ginosar, Kate Rakelly, Sarah Sachs, Brian Yin, and Alexei A Efros. A century of portraits: A visual historical record of american high school yearbooks. In *IEEE International Conference on Computer Vision Workshops (ICCVW)*, pages 1–7, 2015. 2
- [8] James Hays and Alexei A Efros. IM2GPS: estimating geographic information from a single image. In *IEEE Conference on Computer Vision and Pattern Recognition (CVPR)*, pages 1–8, 2008. 2
- [9] Kaiming He, Xiangyu Zhang, Shaoqing Ren, and Jian Sun. Identity mappings in deep residual networks. In *European Conference on Computer Vision (ECCV)*, pages 630–645, 2016. 4, 5
- [10] Alex Hern. *'fishwrap' fake news campaign recycles old news of terror attacks*. In *The Guardian. Online*, 2019. 1
- [11] Gao Huang, Zhuang Liu, Laurens Van Der Maaten, and Kilian Q Weinberger. Densely connected convolutional networks. In *IEEE Conference on Computer Vision and Pattern Recognition (CVPR)*, pages 4700–4708, 2017. 5
- [12] Minyoung Huh, Andrew Liu, Andrew Owens, and Alexei A Efros. Fighting fake news: Image splice detection via learned self-consistency. In *European Conference on Computer Vision (ECCV)*, pages 101–117, 2018. 1
- [13] Nathan Jacobs, Nathaniel Roman, and Robert Pless. Consistent temporal variations in many outdoor scenes. In *IEEE Conference on Computer Vision and Pattern Recognition (CVPR)*, pages 1–6, 2007. 4
- [14] Yong Jae Lee, Alexei A Efros, and Martial Hebert. Style-aware mid-level representation for discovering visual connections in space and time. In *IEEE International Conference on Computer Vision (ICCV)*, pages 1857–1864, 2013. 2
- [15] Pravin Kakar and N Sudha. Verifying temporal data in geotagged images via sun azimuth estimation. *IEEE Transactions on Information Forensics and Security (TIFS)*, 7(3):1029–1039, 2012. 2
- [16] Diederik P Kingma and Jimmy Ba. Adam: A method for stochastic optimization. *arXiv preprint arXiv:1412.6980*, 2014. 4
- [17] Pierre-Yves Laffont, Zhile Ren, Xiaofeng Tao, Chao Qian, and James Hays. Transient attributes for high-level understanding and editing of outdoor scenes. *ACM Transactions on Graphics (TOG)*, 33(4):149, 2014. 2, 3
- [18] Stefan Lee, Nicolas Maisonneuve, David Crandall, Alexei Efros, and Josef Sivic. Linking past to present: Discovering style in two centuries of architecture. In *IEEE International Conference on Computational Photography (ICCP)*, 2015. 2
- [19] Xiaopeng Li, Wenyuan Xu, Song Wang, and Xianshan Qu. Are you lying: Validating the time-location of outdoor images. In *International Conference on Applied Cryptography and Network Security (ACNS)*, pages 103–123, 2017. 2
- [20] Paul Martin, Antoine Doucet, and Frédéric Jurie. Dating color images with ordinal classification. In *ACM International Conference on Multimedia Retrieval (ACMMR)*, page 447, 2014. 2
- [21] Hyeonwoo Noh, Andre Araujo, Jack Sim, Tobias Weyand, and Bohyung Han. Large-scale image retrieval with attentive deep local features. In *IEEE International Conference on Computer Vision (ICCV)*, pages 3456–3465, 2017. 2
- [22] Frank Palermo, James Hays, and Alexei Efros. Dating historical color images. *European Conference on Computer Vision (ECCV)*, pages 499–512, 2012. 2
- [23] Filip Radenović, Giorgos Tolias, and Ondřej Chum. Fine-tuning cnn image retrieval with no human annotation. *IEEE Transactions on Pattern Analysis and Machine Intelligence (PAMI)*, 41(7):1655–1668, 2018. 2
- [24] Tawfiq Salem, Scott Workman, and Nathan Jacobs. Learning a dynamic map of visual appearance. In *IEEE Conference on Computer Vision and Pattern Recognition (CVPR)*, 2020. 2, 3, 4, 5, 6, 8
- [25] Tawfiq Salem, Scott Workman, Menghua Zhai, and Nathan Jacobs. Analyzing human appearance as a cue for dating images. In *IEEE Winter Conference on Applications of Computer Vision (WACV)*, pages 1–8, 2016. 2
- [26] Karen Simonyan and Andrew Zisserman. Very deep convolutional networks for large-scale image recognition. In *International Conference on Learning Representations (ICLR)*, 2015. 4
- [27] Bart Thomee, David A Shamma, Gerald Friedland, Benjamin Elizalde, Karl Ni, Douglas Poland, Damian Borth, and Li-Jia Li. YFCC100M: The new data in multimedia research. *Communications of the ACM*, 59(2):64–73, 2016. 4
- [28] Tsung-Hung Tsai, Wei-Cih Jhou, Wen-Huang Cheng, Min-Chun Hu, I-Chao Shen, Tekoing Lim, Kai-Lung Hua, Ahmed Ghoneim, M Anwar Hossain, and Shintami C Hidayati. Photo sundial: estimating the time of capture in consumer photos. *Neurocomputing*, 177:529–542, 2016. 2
- [29] Sirion Vittayakorn, Alexander C Berg, and Tamara L Berg. When was that made? In *IEEE Winter Conference on Applications of Computer Vision (WACV)*, pages 715–724, 2017. 2
- [30] Anna Volokitin, Radu Timofte, and Luc Van Gool. Deep features or not: Temperature and time prediction in outdoor scenes. In *IEEE Conference on Computer Vision and Pattern Recognition Workshops (CVPRW)*, pages 63–71, 2016. 3
- [31] Tobias Weyand, Ilya Kostrikov, and James Philbin. Planet-photo geolocation with convolutional neural networks. In *European Conference on Computer Vision (ECCV)*, pages 37–55, 2016. 2
- [32] Matthew D Zeiler and Rob Fergus. Visualizing and understanding convolutional networks. In *European Conference on Computer Vision (ECCV)*, pages 818–833, 2014. 6, 7
- [33] Menghua Zhai, Tawfiq Salem, Connor Greenwell, Scott Workman, Robert Pless, and Nathan Jacobs. Learning geo-

- temporal image features. In *British Machine Vision Conference (BMVC)*, 2018. 3
- [34] Bolei Zhou, Agata Lapedriza, Aditya Khosla, Aude Oliva, and Antonio Torralba. Places: A 10 million image database for scene recognition. *IEEE Transactions on Pattern Analysis and Machine Intelligence (PAMI)*, 40(6):1452–1464, 2017. 4, 8
- [35] Peng Zhou, Xintong Han, Vlad I Morariu, and Larry S Davis. Learning rich features for image manipulation detection. In *IEEE Conference on Computer Vision and Pattern Recognition (CVPR)*, pages 1053–1061, 2018. 1